

**Original Article**

**SYNTHESIS OF UREA AND MAGNETITE-BASED CHITIN AS ADSORBENTS FOR THE REMOVAL OF AMLODIPINE BESYLATE**

**CESAR LONDONO, KELLY BARRERA, JOHN ROJAS\* **

School of Pharmaceutical and Food Sciences, University of Antioquia, Street-6753108, Medellin, Columbia  
\*Email; jrojasca@gmail.com

Received: 24 Jun 2023, Revised and Accepted: 21 Jul 2023

**ABSTRACT**

**Objective:** Development of urea and magnetite-based chitin adsorbents for the removal of amlodipine besylate.

**Methods:** Amlodipine is a calcium channel blocker widely used to treat hypertension and angina. However, it is important to treat the residues before disposal so they do not pollute the effluent water sources. The amlodipine sorption property of chitin-based subtract (CBS) was improved by treatment with magnetite and urea, followed by pyrolysis at 500 °C. The FT-IR characterization, elemental composition, pore properties, and sorption isotherms were also assessed.

**Results:** The sorption capacity of amlodipine increased from 4.6 to 9.3 mg/g for the urea and magnetite-treated products, respectively. Further, modified chitin products showed a pore volume (micro and mesopore composition), pore percentage, and roughness of 0.01 cm<sup>3</sup>g<sup>-1</sup>, 0.02 cm<sup>3</sup>g<sup>-1</sup>, 32% and 68%, and 1.2, respectively. The CBS and derivatives did not present Langmurian behavior, indicating a characteristic heterogeneous surface and the presence of energetically distinct sorption sites. The sorption equilibrium was achieved within 5 min, resulting in a net physical sorption.

**Conclusion:** The insertion of nitrogen and iron moieties on the surface of chitin improved the adsorption capacity of amlodipine.

**Keywords:** Chitin, Amlodipine, Urea, Iron oxide, Adsorption

© 2023 The Authors. Published by Innovare Academic Sciences Pvt Ltd. This is an open access article under the CC BY license (<https://creativecommons.org/licenses/by/4.0/>)  
DOI: <https://dx.doi.org/10.22159/ijpps.2023v15i9.48685>. Journal homepage: <https://innovareacademics.in/journals/index.php/ijpps>.

**INTRODUCTION**

Currently, the pharmaceutical industry is becoming one of the major contributors to the pollution of aquatic ecosystems due to the disposal of untreated or unused drugs. Most of these molecules are not biodegradable and cause serious disorders in aquatic organisms. Amlodipine besylate (AB) is one of those drugs that qualifies as an emergent pollutant. It is highly prescribed and used to treat angina and hypertension [1]. Its mechanism of action is related to the inhibition of the initial entry of calcium, which decreases the contractile activity of arterial smooth muscle cells and produces vasodilation. These vasodilator effects lead to a decrease in blood pressure [2]. It is estimated that 30% and 44% of the US and EU populations suffer from hypertension, respectively. Further, it is expected that by 2025, about 1.5 billion people will suffer from hypertension. However, one part of AB is partially metabolized, whereas 6% is excreted unchanged in urine [3]. This drug is partially eliminated in wastewater treatment plants, resulting in low amounts in soil, surface, and ground waters. For instance, AB has been found in waste water from Portugal at levels of 14.9–85.7 ng/l, whereas in effluent waters from hospitals, it was larger (45.5–195 ng/l). Interestingly, in developed countries such as the USA and Canada, it has been found at dangerous levels of 22.9 mg/l [4]. It is also known that levels larger than 10 mg/l cause inhibition of the regeneration of hypostome tentacles and feet in *Hydra vulgaris* [5]. Many types of technologies, such as ion exchange, precipitation, adsorption, reverse osmosis, and solvent, are available to treat wastewater of industrial origin. However, adsorption is still the simplest and most economical technique to undertake since it does not produce any further metabolites. Adsorption implies the accumulation of substances on the surface of a solid or liquid material. Some approaches have been carried out for the production of cheaper and more efficient adsorbents from waste from agricultural production as an adsorbent surface in the purification processes of contaminated water to reduce drug levels [6].

Among these, polysaccharides such as chitin, cellulose, and lignin show remarkable interest. These polymers exhibit special

physicochemical properties, good chemical stability, and particular selectivity towards complex drugs due to the presence of moieties that create ionic interactions with the polymer chains [7]. Further, cellulose and chitin are the two most abundant biopolymers in nature, being renewable and biodegradable. Particularly, chitin, which is obtained from shrimp waste, possesses an acetamide moiety and can be employed for the removal of complex drugs such as AB. Furthermore, it has some advantages over other materials since this natural polymer has favorable characteristics such as biodegradability, non-toxicity, and contaminant adsorption [8]. There is a recent study on the adsorption of AB onto the surface of tosyl carbon nanoparticles containing sulfonate moieties [9]. To our knowledge, there have been no studies conducted on the chemical derivatization of chitin isolated from shrimp waste for the adsorption of AB. Such derivatizations are important to enhance the sorption capacity of chitin.

**MATERIALS AND METHODS**

**Materials**

Shrimp waste was obtained from fishermen on the Pacific coast of Tumaco; sodium hypochlorite and hydrochloric acid were obtained from Qumicos LM (Medellin, Columbia). Nitrogen (99.995% purity) was obtained from Cryogas (Medellin, Colombia). Magnetite was purchased from Sigma Aldrich (St. Louis, Missouri, USA). Acetic acid and potassium hydroxide were obtained from Merck (Darmstadt, Germany), whereas urea was purchased from Supelco (St. Louis, Missouri, USA). Na<sub>2</sub>CO<sub>3</sub> and NaHCO<sub>3</sub> were purchased from Qumicos LM (Medellin, Columbia).

**Preparation of bioadsorbents**

Shrimp waste (500 g) was dried and milled using a knife mill (Willey Arthur Thomas Co., Philadelphia, USA) until a particle size of less than 150 m was obtained. It was then treated with 15% sodium hypochlorite for 5 d to prevent microbial growth. The dispersion was then washed, neutralized with 1.0 mol/l HCl, washed with distilled water, and sonicated at 40 °C for 30 min (E 15H, ELMA,

Elmasonic, Germany) under constant stirring. The material was then vacuum filtered and dried at 100 °C for 24 h in an oven (U30Memmert, Schwabach, Germany). The dried material was passed through a 200 mesh sieve (75 m size) and labeled as CBS.

Pyrolysis of CBS was conducted on a muffle furnace (KSY-6D-16B, Electric Furnace Factory, France) coupled to a 99.995% purity nitrogen source and heated at a rate of 5.0 °C/min up to 500 °C. This temperature remained constant for 2 h under a nitrogen atmosphere pumped at 240 ml/min. Subsequently, the muffle furnace was cooled down, maintaining a constant flow of nitrogen to avoid oxidation of the sample. The resulting material was passed through a 200 mesh (75µm). Approximately, 5 g of magnetite was diluted in 0.5 l of deionized water. Concomitantly, a suspension of 10 g of the pyrolyzed material was dispersed in 0.05 l of CH<sub>3</sub>COOH 1% and added to the magnetite dispersion. This dispersion was then sonicated (Vibra Cell model, Sonics brand, Church Hill Rd., Newtown, Connecticut, USA) in a Rosett homogenization cell at a frequency of 24 kHz and amplitude of 40% in five cycles of 4 min each. The suspension was washed with distilled water, vacuum filtered and the resulting material was submitted to pyrolysis at 500 °C as described previously and labeled as CAM [10].

In a separate experiment, the modified method of Qiao and collaborators was employed for the functionalization of CBS with urea [11]. Approximately 5g of pyrolyzed material was poured into a crucible and mixed with ~15g of urea previously dissolved in 0.050 l of a 5% CH<sub>3</sub>COOH solution under constant stirring. A lid was placed on top of the crucible and introduced into the muffle furnace that was operated under the same conditions as described above. The resulting material was neutralized with 0.1 N KOH to eliminate the excess urea. The material was then washed with hot water, vacuum filtered, dried in an oven at 100 °C for 48 h, passed through 200 mesh sieve (75µm), and labeled as CA1:3U.

#### Chemical characterization of bioadsorbents

The Boehm titration was conducted on ~0.1 g of each sample and 0.025 l of 0.1 mol/l NaOH; 0.05 mol/l Na<sub>2</sub>CO<sub>3</sub>, 0.05 mol/l NaHCO<sub>3</sub> and 0.1 mol/l HCl were then added separately. Subsequently, each solution was shaken for 24 h using a shaker (E 15H, Elmasonic, ELMA, Germany) and 0.005 l aliquots were taken and filtered using a 0.45 µm filter. NaOH and carbonate-treated solutions were titrated with 0.1 mol/l HCl using phenolphthalein and bromocresol green as indicators, respectively. The 0.1 mol/l HCl solution was titrated with 0.05 mol/l NaOH using phenolphthalein as indicator [12].

The IR characterization was conducted on a FT-IR spectrophotometer (Nicolet, Thermo Fisher Scientific, Waltham, Massachusetts, USA) coupled with ATR (Attenuated Total Reflectance) device with readings in a range between 2000 and 600 cm<sup>-1</sup> and 16 Scans. Each sample was placed directly on the sample port without any previous treatment.

#### Specific surface area and pore size distribution

A quantasorb equipment (Nova 1200e, Quantachrome, Boynton Beach, USA) was employed with nitrogen gas as adsorbate. Samples were subjected to 250 °C for 4 h, except for CBS, which was subjected to 150 °C under vacuum (15 mmHg). The sorption isotherms were used to determine the total pore volume V<sub>tot</sub> (calculated from nitrogen uptake at the relative pressure of 0.95), total micropore and mesopore volumes according to the Distribution Functional Theory method. Pore size distribution and pore radius were also determined. Further, the fractal dimension (DF) was calculated by the Frenkel-Halsey-Hill (FHH) method on the desorption isotherms [13].

#### Point of zero charge

Approximately 0.01 g of each material was weighed separately in 0.01 l of different aqueous solutions having several pH values (i. e, 2, 4.3, 6.6, 8.2, 10.3, and 12.0). The readings were made on a ZetaSizer (Nano-ZS90 Series, Malvern Instruments Ltd., UK) using the ZetaSizer software, version 7.10. Quantification was done in triplicate at 25 °C with an equilibrium time of 2 min. The PZC was calculated by plotting the pH of each sample as a function of mV. The

PZC corresponds to the point where the curve intercepts the X axis, reaching a neutral surface charge [14].

#### Amlopidine besylate (AB) adsorption measurements

Approximately 0.02 g of each material was taken and 0.025 l of a 4.1, 16.4, 25 and 35 mg/l solutions of AB was added. Samples were then stirred for 1 h at 300 rpm at room temperature and settled down for 30 min, followed by filtration with a 0.22 µm filter. Adsorption data were fitted to several non-linear sorption models. The Elovich isotherm establishes that sorption increases exponentially with the adsorption sites through a type of multilayer adsorption [15]. This model is expressed as follows:

$$Q_e = A * K * C_e * \exp\left(-\frac{Q_e}{A}\right) \quad (1)$$

Where, A corresponds to the maximum adsorption capacity (mg/g) and K (Lg<sup>-1</sup>) corresponds to the adsorption constant.

The Freundlich model shown in equation 2 also explains the adsorption process for a heterogeneous surface, where the high energy adsorption sites are occupied first, forming multilayers [16].

$$Q_e = K * C_e^{\frac{1}{n}} \dots\dots\dots (2)$$

Where, Q<sub>e</sub> is the equilibrium adsorption, K (mg/g) and 1/n correspond to the adsorption capacity and the relative distribution of energy (heterogeneity) of the adsorbent sites. Thus, 1/n>1 indicates cooperative adsorption, 1/n<1 corresponds to a normal adsorption and 1<n<10 indicates a favorable adsorption process [17].

The Dubinin-Radushkevich model is used to predict whether the adsorption is physisorption or chemisorption by calculating the activation energy. This model was developed to quantify the effect of the pore structure of the adsorbents and assumes that the adsorption process is related to the filling of the micropore volume, as opposed to layer-by-layer adsorption on the pore walls [18]. This model does not consider a homogeneous surface and is expressed as follows:

$$Q_e = Q_{max} e^{-(\beta \cdot \epsilon^2)} \dots\dots (3)$$

Where Q<sub>e</sub> is the amount of adsorbent adsorbed per unit mass of adsorbent at equilibrium (mg g<sup>-1</sup>), Q<sub>max</sub> corresponds to the saturation adsorption capacity (mg g<sup>-1</sup>), β is a constant related to the free adsorption energy (mol<sup>2</sup>kJ) and ε is the Polanyi adsorption potential (kJ mol<sup>-1</sup>) and it is expressed as:

$$\epsilon = RT \ln\left(1 + \frac{1}{C_e}\right) \dots\dots\dots (4)$$

Where C<sub>e</sub> is the equilibrium adsorbate concentration in solution. R corresponds to the universal gas constant (8.314 Jmol<sup>-1</sup> K<sup>-1</sup>) and T is the absolute temperature (298.15K). The mean adsorption energy is found by:

$$E = \frac{1}{\sqrt{2\beta}} \dots\dots\dots (5)$$

If this activation energy is less than 8 kJmol<sup>-1</sup> the process is physical, but values between 8 and 16 kJ mol<sup>-1</sup> correspond to chemisorption [19, 20].

The adsorption rates and the corresponding parameters were found by the pseudo-second and Avrami models. The pseudo-second-order kinetic model describes that the rate of occupancy of adsorption sites is proportional to the square of the number of unoccupied active adsorption sites, as follows:

$$Q_t = Q_e \left[1 - \frac{1}{(1+(k \cdot t))}\right] \dots\dots\dots (6)$$

Where k is the pseudo-second-order adsorption constant (g mg<sup>-1</sup> min<sup>-1</sup>). The Avrami kinetics applies to reaction and crystallization kinetics. This model is expressed as follows:

$$Q_t = Q_e [1 - e^{-k \cdot t}]^n \dots\dots\dots (7)$$

Where k (min<sup>-1</sup>) corresponds to the kinetics rate and depends on the geometry of the sorption site, whereas the time exponent indicates the change in the adsorption mechanism. N is equal to 0.5

for diffusion-driven processes, whereas for a phase boundary adsorption,  $n$  is  $\sim 1$ .

## RESULTS AND DISCUSSION

The FT-IR spectra of all materials are depicted in fig. 1. The different signals and their respective wave number allow assigning the functional groups present in the adsorbent and determining the changes that occur in the materials after each physicochemical modification [21]. The CBS shows two bands at 1191  $\text{cm}^{-1}$  and 895  $\text{cm}^{-1}$ , which are common for chitin samples having a small degree of deacetylation, and these two bands correspond to the  $\beta$  1-4 linkage.

The bands at 1650  $\text{cm}^{-1}$  and 1557  $\text{cm}^{-1}$  correspond to the acetamide group of type I amide and type II NH torsion. Likewise, the bands at 1329  $\text{cm}^{-1}$  and 1377  $\text{cm}^{-1}$  are typical of type III amide and stretching vibrations of the methyl group of the acetamide groups. The peak at 1427  $\text{cm}^{-1}$  is attributed to the symmetrical bending of  $\text{CH}_2$ , whereas the peak at 1255  $\text{cm}^{-1}$  corresponds to the C-O-H bending, and the peak at 1161  $\text{cm}^{-1}$  corresponds to the symmetrical stretching C-O-C ( $\beta$ -glycosidic linkage). The peak at 1063  $\text{cm}^{-1}$  is due to C-O/C-C stretching and the band at 895  $\text{cm}^{-1}$  corresponds to the asymmetric out-of-plane stretching of the  $\beta$ -glycosidic carbon.

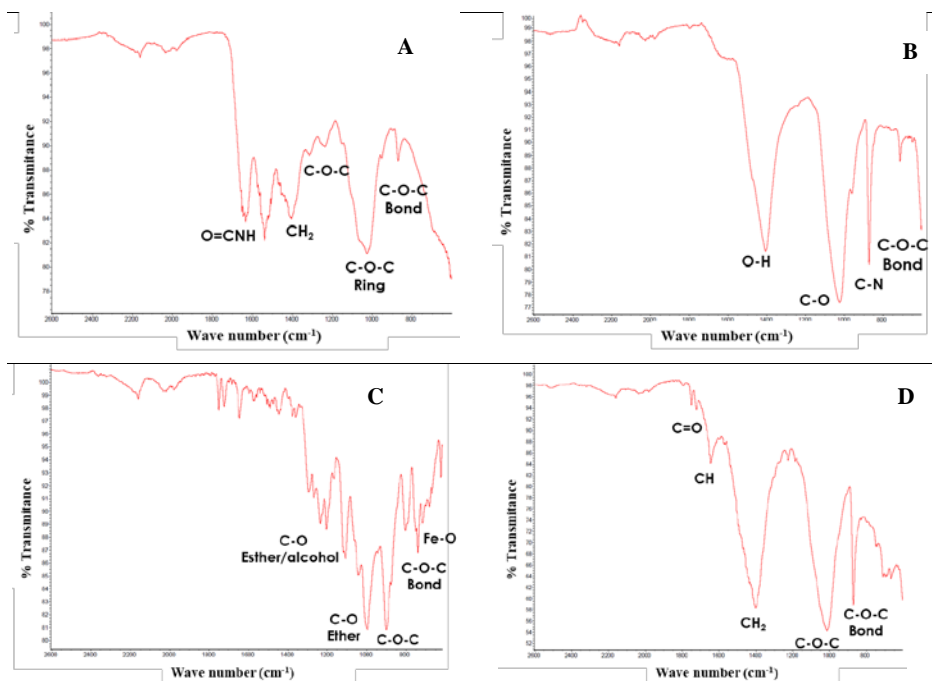


**Fig. 1:** FT-IR infrared spectra of different adsorbents. (A) Chitin-based substrate, CBS (B) urea-treated material, CA1:3U, (C) magnetite-treated material, CAM, (D) commercial activated carbon, CAC

The pyrolysis process along with urea activation, decreased the macrostructure of chitin as depicted in fig. 1b since the- $\text{CH}_2$  stretching at 1400  $\text{cm}^{-1}$  and the C-O-C signal at  $\sim 850$   $\text{cm}^{-1}$  decreased. The loss of carbon could also be associated to the loss of hydrogen, oxygen, and nitrogen as  $\text{CO}_2$  or  $\text{NO}_2$ , leaving behind a rigid carbon skeleton. Further, treatment with urea led to the disappearance of the signals related to the C=O and C=N stretching at 1680  $\text{cm}^{-1}$  and 1590  $\text{cm}^{-1}$ , respectively, as observed in the CBS. Similarly, a 6-fold increase was observed for the C-O and C-N bands.

Fig. 1c depicts the FT-IR spectrum of the magnetite-treated material. Sonication allowed for particle disaggregation and breakdown of particulate matter. Once pyrolysis took place, iron (III) was deposited on the surface of the carbonaceous structure. Thus, new signals emerged at 1200  $\text{cm}^{-1}$  corresponding to the C-O stretching. The band at 1113  $\text{cm}^{-1}$  corresponded to the C-O-C linkage; whereas those bands at 720  $\text{cm}^{-1}$  and 790  $\text{cm}^{-1}$  are attributed to the Fe-O vibrations. Further, the band at 1645  $\text{cm}^{-1}$  is attributed to Fe-OH stretching. The peak at 610  $\text{cm}^{-1}$  is assigned to Fe-O of iron oxide ( $\text{Fe}_2\text{O}_3$ ). The weak bands at 1502  $\text{cm}^{-1}$  and 1415  $\text{cm}^{-1}$  correspond to the C=C stretch, whereas those peaks at 815  $\text{cm}^{-1}$  and 675  $\text{cm}^{-1}$

are related to C-C stretching [22]. Even though the starting material was magnetite, the resulting modified product showed the presence of hematite-type ferric oxide, which indicates oxidation during the pyrolysis process. On the other hand, the FT-IR spectrum of commercial activated carbon (fig. 1d), showed bands between 1640-1750  $\text{cm}^{-1}$  which are attributed to C=O and C-O of the phenolic ester and conjugated ketone structures. Likewise, the intensity of the  $\text{CH}_2$  band at  $\sim 1400$   $\text{cm}^{-1}$  shows that cyclic structures predominate in this material. Further, several bands related to aromatic rings were also observed between 700 and 900  $\text{cm}^{-1}$ [23].

Table 1 shows the physicochemical properties of the materials. The alkaline nature of chitin increased in the resulting functionalized materials. Further, the number of acid moieties also increased, whereas the phenolic groups tend to decrease. The resulting pH of the aqueous solution of these materials was alkaline in nature. Functionalization with urea and magnetite also contributed to the increase in surface area and led to a decrease in particle size, possibly due to the synergistic effect of pyrolysis. Except for CAC, the specific surface area of CBS and its derivatives had little contribution to the adsorption capability.

**Table 1:** Physicochemical characterization of the adsorbents

Material	Total acidity	Boehm titration ( $\mu\text{mol g}^{-1}$ )			Total alkalinity	Surface Area ( $\text{m}^2\text{g}^{-1}$ )	PZC value	Yield (%)	pH	Conductivity ( $\mu\text{S cm}^{-1}$ )	Particle size ( $\mu\text{m}$ )
		Phenol	Lactone	Acid groups							
CBS	3960	3960	0	0	5850	10.2	2.5	81.7	9.1	271	36.5
CA1:3U	10610	3880	0	6720	9970	22.9	2.3	97.7	9.1	167	7.5
CAM	9120	2370	0	6730	9820	20.2	2.3	84.1	8.7	74	5.8
CAC	4320	4320	0	0	950	243.0	3.8	N/A	7.0	3268	12.2

Fig. 2 shows SEM micrographs of the materials at, 2000x magnification. The CBS shows an irregular morphology of particles with slightly rough and planar surfaces, where some small crystals of sodium chloride appear on the surface and were not completely removed during the washing processes. CAM was composed of regular particles with a very rough surface composed essentially of ferric oxide (III) nanoparticles, whereas CA1:3U was composed of irregular particles similar to those of CBS where the surface was

slightly rough. The iron nanoparticles exhibited a snowflake shape, having ~ 50-100 nm in size. On the other hand, the CAC was composed of particles with a greater number of edges and flat surfaces. These morphological characteristics allow it to be classified as the most important adsorbent in nature, which can house many chemical compounds, such as drugs, heavy metals, dyes, among others. In addition, these properties allow its use in the pharmaceutical field, and it is used as an antidote in drug poisoning [24].

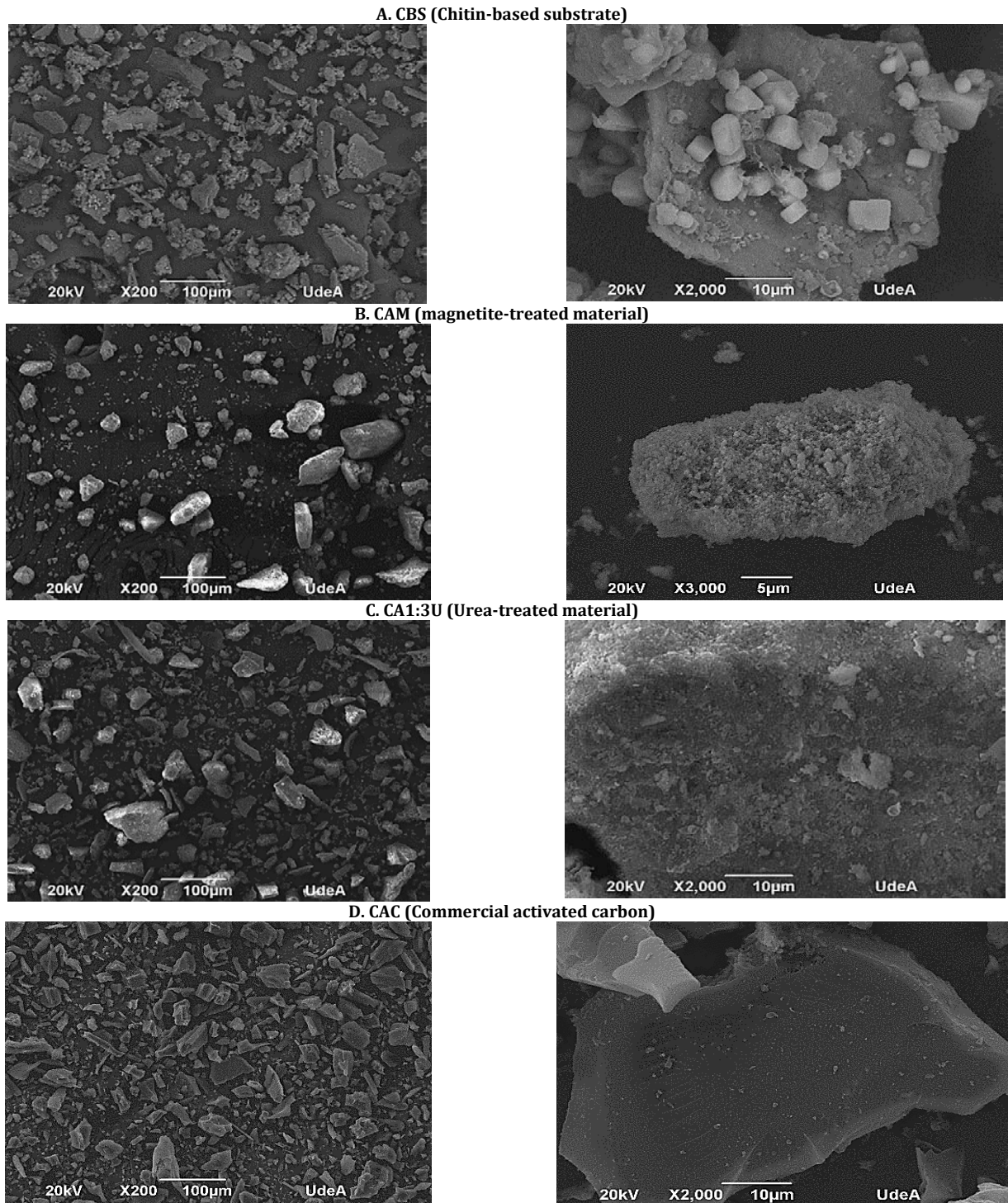


**Fig. 2: SEM micrographs of CBS (A), CAM (B), CA1:3U (C) and CAC (D)**

The N<sub>2</sub> sorption isotherms are depicted in fig. 3. The adsorbed volume of nitrogen was much higher in the CAC followed by

CAM, whereas the CBS and CA1:3U did not show significant differences.

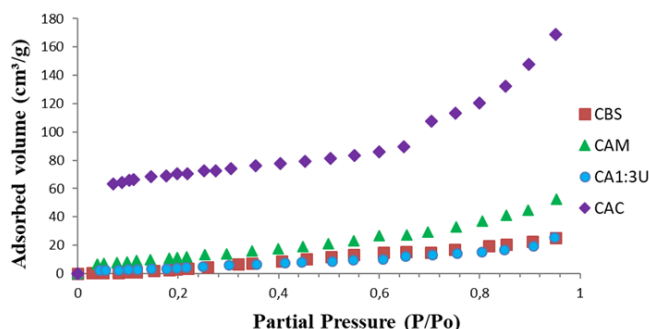


Fig. 3: N<sub>2</sub> isotherms of the adsorbents

The CAC showed a type I isotherm shape, which is limited to adsorption in monomolecular layers, especially for microporous materials having high adsorption at low pressures. The other three materials showed a type II isotherm shape common for materials having monolayers and multilayers with an inflection

point where the completion of the monolayer occurs. Pore characterization parameters are listed in table 2. The functionalized material with iron had a drastic change in the pore structure, having a more microporous system similar to that of CAC.

Table 2: Pore size characterization

Property	Parameter	CBS	CAM	CA1:3U	CAC
Accumulated pore volume (cm <sup>3</sup> g <sup>-1</sup> )	Micropore (<20Å)	0.01	0.02	0.01	0.08
	Mesopore (20-500Å)	0.02	0.06	0.02	0.16
Pore amount (%)	Micropore (<20Å)	46.9	32.1	32.4	35.8
	Mesopore (20-500Å)	53.1	67.9	67.6	64.2
Functional distribution theory (DFT)	Pore volume (cm <sup>3</sup> g <sup>-1</sup> )	0.03	0.07	0.04	0.22
	Pore diameter (Å)	14.5	13.9	22.7	6.4
Fractal dimension (D)	Excluding surface tension effects	0.7	1.2	1.5	2.3
	Including surface tension effects	2.2	2.4	2.5	2.8

The fractal dimension (FD) describes the topography of the surfaces and quantifies the actual surface roughness showing the following trend: CAC>CAM>CA1:3U>CBS, which agrees with the ranking of pore volume and pore diameter. It is also observed that the values of FD, including the surface tension of N<sub>2</sub> were larger in magnitude.

Table 3 and fig. 4 show data fitting to the adsorption kinetics of AB. Functionalized materials such as CAM and CA1:3U showed the best fit to the pseudo-second-order model, which describes that the rate of occupation of the adsorption sites is related to the square of the number of unoccupied adsorption sites. This means a fast initial rate of k values of ~0.84 mg g<sup>-1</sup> min<sup>-1</sup>, whereas reported values for nano adsorbents such as Ag-TiO<sub>2</sub> showed values of 2.35 mg g<sup>-1</sup> min<sup>-1</sup>, requiring longer treatment times [25]. Usually, materials having good fit to such kinetic model involve small and simple adsorbate species because they tend to diffuse rapidly in solution, adopting different molecular conformations within tiny pore spaces in

fractions of seconds. In this case only such collisions that imply collisions with two unoccupied sites at once are taken into account, resulting in sticking [26]. It is possible that sticking takes place at individual sites composed of two or more functional groups at the surface of the adsorbents, such as Fe (III) and N.

Likewise, the CBS and CAC materials presented the best fit to the Avrami model. In this case, the adsorption process might have a rapid initial fast first stage due to a mass transfer of adsorbate from the aqueous solution to the material surface followed by a slow phase where migration of the drug within the pores and capillary spaces of the sorbent took place. Independent of the model used, CBS presented the lowest Q<sub>e</sub> values, indicating that chemical modification improved the adsorption of AB. Further, a rapid AB was also observed, indicating in most cases that Q<sub>e</sub> was reached within 5 min. Further, the time-related constants such as “K” and “n” did not show major differences among all materials due to the rapid adsorption process.

Table 3: Parameters resulting from amlodipine adsorption kinetics models

Model	Parameter	CBS	CAM	CA1:3U	CAC
Avrami	Q <sub>e</sub> (mg g <sup>-1</sup> )	4.3	8.6	8.5	8.5
	K (min <sup>-1</sup> )	3	3	3	3
	n	1	1	1	1
	r <sup>2</sup> Adjusted	0.90	0.91	0.88	0.90
Pseudo 2 <sup>nd</sup> Order	Q <sub>e</sub> (mg g <sup>-1</sup> )	4.6	9.3	9.3	9.2
	K (mg g <sup>-1</sup> min <sup>-1</sup> )	0.82	0.84	0.84	0.84
	r <sup>2</sup> Adjusted	0.80	0.98	0.98	0.87

Table 5 and fig. 5 show the parameters resulted from the adsorption isotherms. CBS shows the best fit to the Freundlich model, which states that the adsorption sites on the surface of the adsorbent are energetically heterogeneous, with those with the highest energy being occupied first and the possible formation of multilayers. Similar studies conducted on carbon nanotubes and lipophilic drugs such as betamethasone showed “n” and “k” values of 0.7 and 5.1 mg

g<sup>-1</sup>, respectively. This could be explained by the large surface area and hydrophobic character of the carbon nanotubes [27]. On the other hand, CAC and CAM presented a good fit to the Elovich model, which describes that the adsorption increases exponentially with the available multilayer adsorption sites [28]. CA1:3U presented the best data fit to the Dubinin-Radushkevich model, which also applies to heterogeneous surfaces.

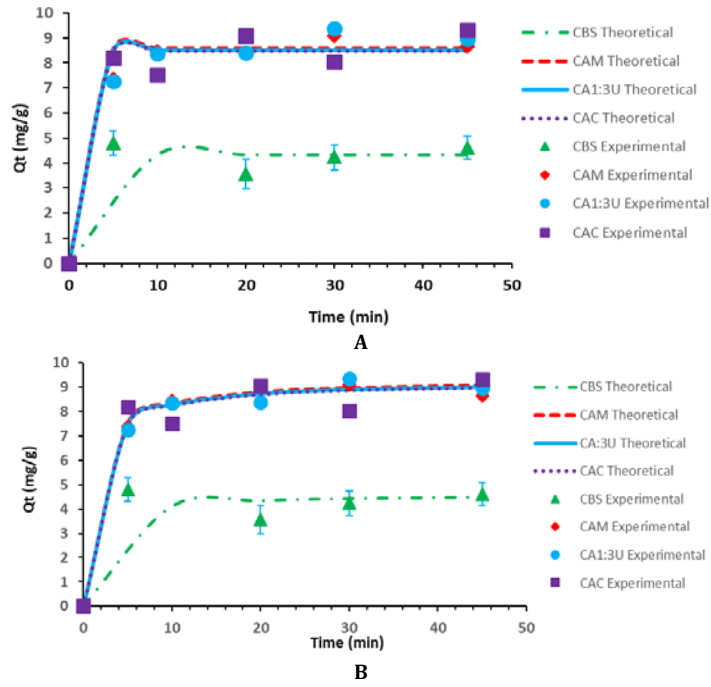


Fig. 4: Amlodipine adsorption kinetics fitted to the Avrami (A) and pseudo-second-order (B) models

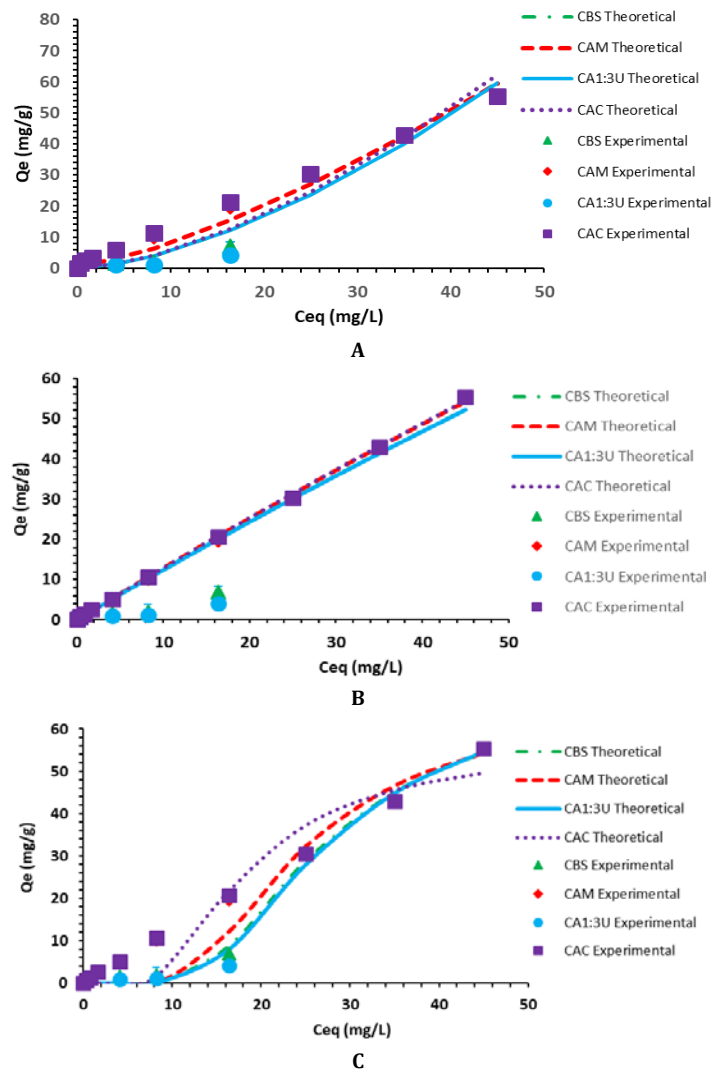


Fig. 5: Amlodipine isotherms according to the Freundlich (A), Elovich (B) and Dubinin-radushkevich (C) models

Table 5: Parameters resulting from amlodipine isotherm models

Model	Parameter	EE	CAM	CA1:3U	CAC
Freundlich	k (mg g <sup>-1</sup> )	0.14	0.38	0.14	0.77
	n	0.63	0.75	0.63	0.88
	r <sup>2</sup> Adjusted	1.000	0.890	0.769	0.9540
Elovich	A (mg g <sup>-1</sup> )	525.6	548.2	524.8	536.7
	K (L g <sup>-1</sup> )	0.002	0.002	0.002	0.002
	r <sup>2</sup> Adjusted	0.584	0.994	0.421	0.995
Dubinin-Radushkevich	Q <sub>max</sub> (mg g <sup>-1</sup> )	43.2	42.3	42.7	67.2
	β (mol <sup>2</sup> kJ <sup>-2</sup> )	14.7	29.8	28.8	73.8
	E (kJ mol <sup>-1</sup> )	0.19	0.23	0.13	0.08
	r <sup>2</sup> Adjusted	0.531	0.680	0.791	0.536

Fig. 6 shows the infrared spectra of each of the materials after carrying out the AB adsorption process. These results proved these materials interact with AB via ionic interactions and hydrogen bonding through physisorption. Further, the Dubinin-Radushkevich model also proved that adsorption took place by a

physical process since values of energy were lower than 8 kJ mol<sup>-1</sup>. AB exhibits a high pKa of ~8.6, and at experimental conditions, the amine group should be positively charged, easing the formation of ionic interactions with materials having PZC values < 3.8.

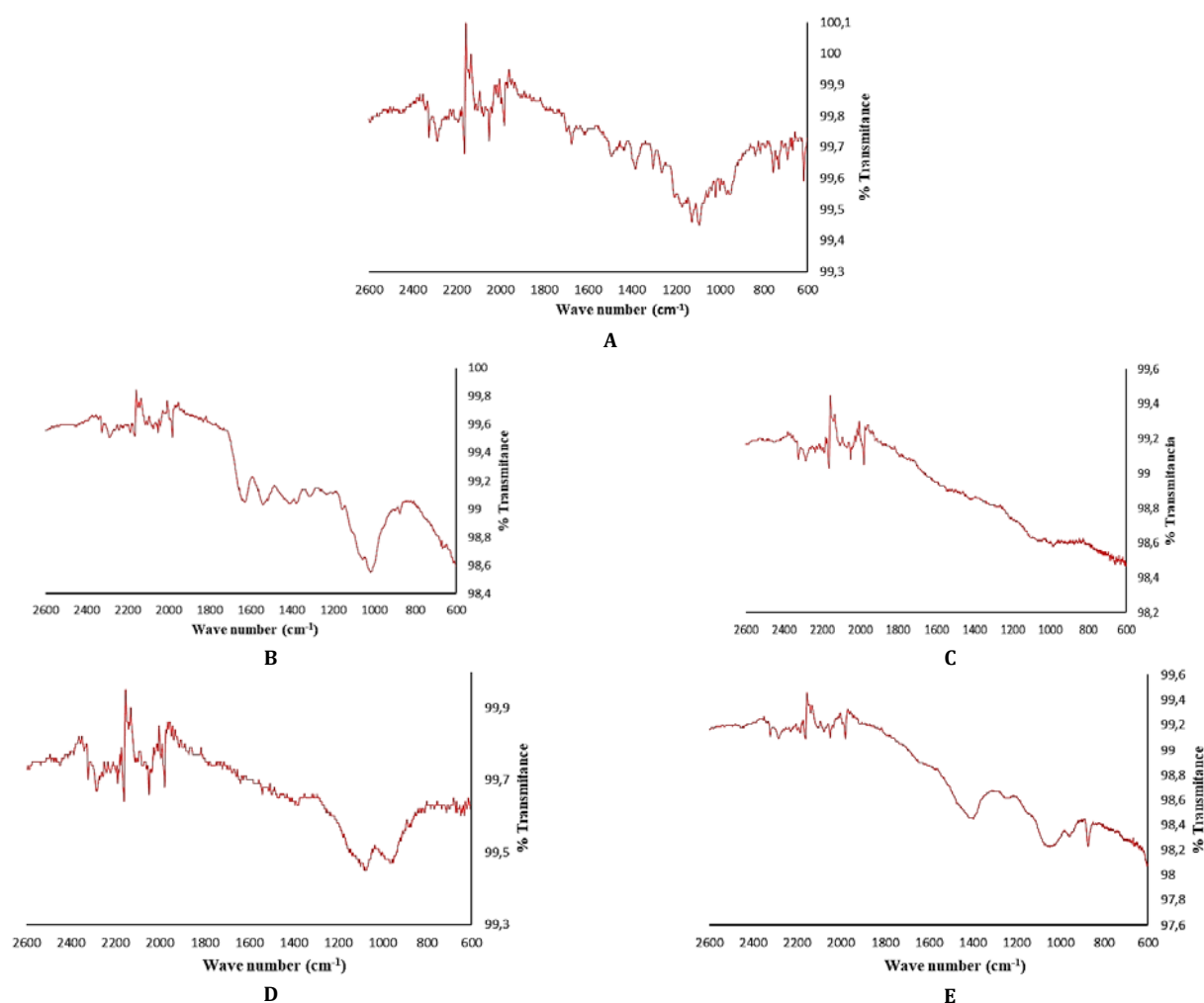


Fig. 6: Infrared spectra of the bioadsorbents after the adsorption test. AB (A), AB and CBS (B), AB and CAC (C), AB and CAM (D), AB and CA1:3U (E)

## CONCLUSION

The chemical modifications conducted of chitin introduced amine and iron oxide groups on the surface, which was reflected on the sorption capacity of AB as seen by the  $Q_e$  values. The kinetics models showed that  $Q_e$  was reached within 5 min. Likewise, the isotherm modes showed a non-Langmuirian sorption behavior, indicating the prevalence of a heterogeneous surface along with the

formation of multilayers. The sorption process suited to a physical process which was reversible in nature.

## ACKNOWLEDGMENT

The authors thank the Environmental Remediation and Biocatalysis group (GIRAB) of the University of Antioquia for providing the necessary resources to carry out this study.

**FUNDING**

Nil

**AUTHORS CONTRIBUTIONS**

All the authors have contributed equally.

**CONFLICT OF INTERESTS**

The authors declare no conflict of interest.

**REFERENCES**

- Manimaran V, Damodharan N. Development of fast-dissolving tablets of amlodipine besylate by solid dispersion technology using poloxamer 407 and poloxamer 188. *Asian Journal of Pharmaceutical and Clinical Research*. 2017 Apr 10;7:135-41. doi: 10.22159/ajpcr.2017.v10i7.17686
- Bharati AR, Deshmane SV, Biyani KR. Stability indicating rp-hplc method development and validation for simultaneous estimation of amlodipine and hydrochlorothiazide in pharmaceutical dosage form. *Chromatography Research International*. 2015 Sep 10;7(4):79-82. <https://doi.org/10.1155/2014/628319>
- Saxena D, Damale S, Datar A. Study of the *in vitro* metabolic profile of amlodipine in human hepatic cell line and chicken liver tissue using liquid chromatography-mass spectrometry. *J Mass Spectrom*. 2016 May;9(4):365-71.
- Jakimska A, Sliwka Kaszynska M, Nagorski P, Namiesnik J, Kot Wasik A. Phototransformation of amlodipine: degradation kinetics and identification of its photoproducts. *PLoS One*. 2014 Oct;9(10):e109206. doi: 10.1371/journal.pone.0109206, PMID 25279815.
- Patel M, Kumar R, Kishor K, Mlsna T, Pittman CU, Mohan D. Pharmaceuticals of emerging concern in aquatic systems: chemistry, occurrence, effects, and removal methods. *Chem Rev*. 2019 Mar 5;119(6):3510-673. doi: 10.1021/acs.chemrev.8b00299, PMID 30830758.
- Sinbah HJ, Khazaal MH, Hassen HS, Hassan ES. A comparison of kinetic studies of kaolin clay and rice husks for ciprofloxacin adsorption. *Int J App Pharm*. 2023 Apr 03;15(3):132-7. doi: 10.22159/ijap.2023v15i3.46495.
- Chauhan S, Shafi T, Dubey BK, Chowdhury S. Biochar-mediated removal of pharmaceutical compounds from aqueous matrices via adsorption. *Waste Dispos Sustain Energy*. 2023;5(1):37-62. doi: 10.1007/s42768-022-00118-y, PMID 36568572.
- Nerdy N, Lestari P, Simorangkir D, Aulianshah V, Yusuf F, Bakri TK. Comparison of chitosan from crab shell waste and shrimp shell waste as natural adsorbent against heavy metals and dyes. *Int J App Pharm*. 2021 Dec 21;14(2):181-5. doi: 10.22159/ijap.2022v14i2.43560.
- Amiri M, Imanzade H. Adsorption of amlodipine at the surface of tosyl-carbon nanoparticles for electrochemical sensing. *Iran J Pharm Res*. 2016;15(3):303-11. PMID 27980564.
- Samoilova NA, Krayukhina MA. Chitin-based magnetic composite for the removal of contaminating substances from aqueous media. *Russ Chem Bull*. 2020 Jul;69(6):1157-64. doi: 10.1007/s11172-020-2883-7.
- Guan L, Pan L, Peng T, Gao C, Zhao W, Yang Z. Synthesis of biomass-derived nitrogen-doped porous carbon nanosheets for high-performance supercapacitors. *ACS Sustainable Chem Eng*. 2019;7(9):8405-12. doi: 10.1021/acssuschemeng.9b00050.
- Schönherr J, Buchheim J, Scholz P, Adelhelm P. Boehm titration revisited (Part I): Practical aspects for achieving a high precision in quantifying oxygen-containing surface groups on carbon materials. *C - Journal of Carbon Research* 2018 Apr;4(2):2-21.
- Pomonis PJ, Tsaousi ET. Frenkel-halsey-hill equation, the dimensionality of adsorption, and pore anisotropy. *Langmuir*. 2009 Oct;25(17):9986-94. doi: 10.1021/la901121c, PMID 19705894.
- Dai M. The effect of zeta potential of activated carbon on the adsorption of dyes from aqueous solution: I. *Journal of Colloid and Interface Science*. 1994 Apr;164(1):223-8. doi: 10.1006/jcis.1994.1160.
- Dada AO, Olalekan AP, Olatunya AM, Dada O. Langmuir, freundlich, temkin and dubinin-radushkevich isotherms studies of equilibrium sorption of Zn<sup>2+</sup> onto phosphoric acid modified rice husk. *IOSR Journal of Applied Chemistry*. 2012 Dec;3(1):38-45.
- Debord J, Harel M, Bollinger JC, Chu KH. The elovich isotherm equation: back to the roots and new developments. *Chemical Engineering Science*. 2022 Nov;262(23):118012. doi: 10.1016/j.ces.2022.118012.
- Foo KY, Hameed BH. Insights into the modeling of adsorption isotherm systems. *Chemical Engineering Journal*. 2010;156(1):2-10. doi: 10.1016/j.ces.2009.09.013.
- Ramachandran P, Vairamuthu R, Ponnusamy S. Adsorption isotherms, kinetics, thermodynamics and desorption studies of reactive orange 16 on activated carbon derived from ananas comosus (L.) carbon. 2011 Nov 11;6(11):15-26.
- Priya SS, Radha KV. Equilibrium, isotherm, kinetic and thermodynamic adsorption studies of tetracycline hydrochloride onto commercial grade granular activated carbon. *International Journal of Pharmacy and Pharmaceutical Sciences*. 2014 Aug 25;7(1):42-51.
- Hu Q, Zhang Z. Application of dubinin-radushkevich isotherm model at the solid/solution interface: a theoretical analysis. *Journal of Molecular Liquids*. 2019 Mar;277(1):646-8. doi: 10.1016/j.molliq.2019.01.005.
- Singh TP, Cb M. A comparison between biosorption and bioaccumulation of fluoride from wastewater. *Asian J Pharm Clin Res*. 2017 Nov 27;11(3):92-100. doi: 10.22159/ajpcr.2018.v11i3.16604.
- Wan Nor W, Che Soh S, Azmi A, Yusof M, Shamsuddin M. Synthesis and physicochemical properties of magnetite nanoparticles (Fe<sub>3</sub>O<sub>4</sub>) as potential solid support for homogeneous catalysts. *Malaysian Journal of Analytical Sciences*. 2018 Aug;22(5):768-74.
- Cuhadaroglu D, Uygun OA. Production and characterization of activated carbon from a bituminous coal by chemical activation. *African Journal of Biotechnology*. 2008 Oct;7(20):3703-10.
- Hassen JH, Ayfan AH, Farhan YM. Spectroscopic evaluation of activated charcoal as a poison antidote for gliclazide drug. *Asian J Pharm Clin Res*. 2017 Nov 30;11(3):140-3. doi: 10.22159/ajpcr.2018.v11i3.23054.
- Rabhi S, Mahtout L, Bououdina M, Khezami L, Belkacemi H, Kerrami A. Tuning the photocatalytic activity of TiO<sub>2</sub> by Ag loading: experimental and modelling studies for the degradation of amlodipine besylate drug. *Ceramics International*. 2021 Apr 17;47(15):21509-21. doi: 10.1016/j.ceramint.2021.04.162.
- Hubbe A, Azizian S, Douven S. Implications of apparent pseudo-second-order adsorption kinetics onto cellulosic materials: a review martin "adsorption rates review. *BioRes*. 2019 Aug 7;14(3):7582-626.
- Vadi M, Hossinie N, Shekari Z. The adsorption equilibrium isotherms Freundlich, langmuir, and Temkin models for two steroidal anti-inflammatory drugs (NSAIDs) betamethasone and clobetasol on multi-walled carbon nanotube. *Orientjchem*. 2013 Feb 28;29(2):685-90. doi: 10.13005/ojc/290242.
- Singh TP, Cb M. Removal of fluoride using neem leaves batch reactor: kinetics and equilibrium studies. *Asian J Pharm Clin Res*. 2017 Dec 06;11(3):237-41. doi: 10.22159/ajpcr.2018.v11i3.14080.